CHAPTER 3

Key Research Outcomes

During the year, NISE has taken up Research, Development and Demonstration (RD&D) activities in various solar energy technologies through in-house, externally funded, and collaborative projects. These projects are identified in line with the mandate of NISE and have current relevance in catering to the changing needs of the energy sector. Key research outcomes from various projects undertaken by NISE during the year are detailed below:

3.1 A low-cost synthesis process for the production of monosized particles

To enhance the efficiency of nanostructured solar cells, particularly radial junction solar cells, and improve the stability of perovskite solar cells, the PV R&D Laboratory has developed a low-cost, semi-batch synthesis process based on the Stöber method. This method enables the controlled production of monodisperse silica particles ranging from the nanoscale to microscale. By precisely adjusting key reaction parameters—such as precursor, hydrolyzing agent, and catalyst concentrations—the process allows fine-tuning of particle size, morphology, and distribution, which is critical for optimizing performance in advanced solar cell applications.

The method has successfully produced monodisperse silica particles with diameters from 0.67 µm to 3.2 µm, synthesized by varying only the precursor concentration. These particles exhibit sharp absorption in the ultraviolet region, attributed to the presence of E centers—paramagnetic defects associated with positively charged oxygen vacancies (≡Si•Si≡) and dangling bonds (≡Si•). These optically active defects form during particle growth due to incomplete Si-O-Si network formation. The controlled creation of such defect centers and precise tuning of particle properties enhance light absorption and structural compatibility.

In a similar way, variation in the concentration of the hydrolyzing agent and catalyst produced monosized silica particles of varying sizes. Figure 3.1 shows such controlled size variation achieved by varying the concentration of the precursor (TEOS), the hydrolyzing agent (H_2O), and the catalyst (ammonia).

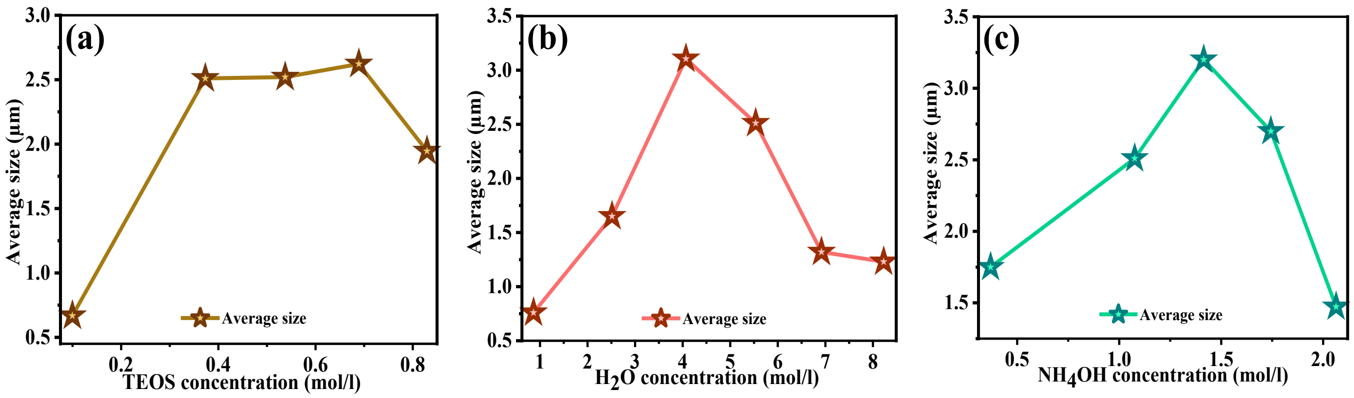

Figure 3.1: Variation of the size of PSPs with the variation of (a) TEOS concentration (0.099 – 0.829 mol/l), (b) H_2O concentration (0.865 – 8.227 mol/l), (c) ammonia concentration (0.369 – 2.064 mol/l) respectively.

The photoluminescence (PL) spectra of the synthesized silica particles exhibit a broad range of emission peaks spanning from the ultraviolet to the red region (280–900 nm), as shown in Figure 3.2. The deconvolution of the PL spectrum shows the presence of several peaks from the UV to the red region. Variations in the concentrations of TEOS, H2O, and ammonia did not show a direct correlation with PL behaviour. However, a clear trend was observed: PL intensity decreased as particle diameter increased. Additionally, a slight blue shift in emission peaks was noted with increasing particle size. The decline in PL intensity with larger particle sizes is attributed to a reduction in the concentration of Oxygen-Deficient Centers (ODCs) on the silica particle surfaces. This interpretation is supported by EDAX analysis, which indicates an increase in oxygen content in larger particles. The higher oxygen content suggests enhanced passivation of surface defects. In particular, defects such as ≡Si–O–S–O–Si≡ (two-fold coordinated silicon) and ≡Si–Si≡ (neutral oxygen vacancy) are increasingly passivated in larger particles. This reduction in active defect sites leads to a diminished PL response, confirming the role of surface ODCs in governing the optical properties of the silica particles.

The observed blue PL peak can be attributed to self-trapped excitons (STEs) undergoing intrinsic radiative decay involving triplet-to-singlet transitions. These excitons are typically generated through high-energy excitation sources such as vacuum UV, UV light, energetic electrons, or multiphoton excitation. Given the wide bandgap of bulk SiO_2 (~11 eV), the use of 200 nm excitation light (corresponding to 12.4 eV from two photons) in the PL study provides sufficient energy to generate free excitons within the silica matrix. As a result, the PL spectra arise from two-photon-induced free exciton generation, followed by energy relaxation through a self-trapping process. This leads to STE-based PL or energy transfer to existing defects and impurities, which then emit their characteristic PL signals. The broad violet-UV emission peak around 410–427 nm, along with a shoulder near 347 nm, is likely due to internal relaxation of localized PL-active oxygen-deficient centers (ODCs), specifically two-fold coordinated silicon species (≡Si–O–Si–O–Si≡). A sharp green PL peak near 494 nm and a shoulder at approximately 534 nm are attributed to hydrogen-related species, such as surface ≡Si–H groups. Emission peaks in the red region are linked to non-bridging oxygen hole centers (NBOHCs), which also contribute to the PL response.

3.2 Fabrication of semi-periodic inverted pyramid array pattern

The monosized silica particles were used as an etching mask to fabricate periodic inverted pyramid structures on the top surface of Si wafers without doing complicated lithographic steps (Figure 3.3 (a)). To achieve such periodic structures first a non-closed pack self-assembled monolayer of silica

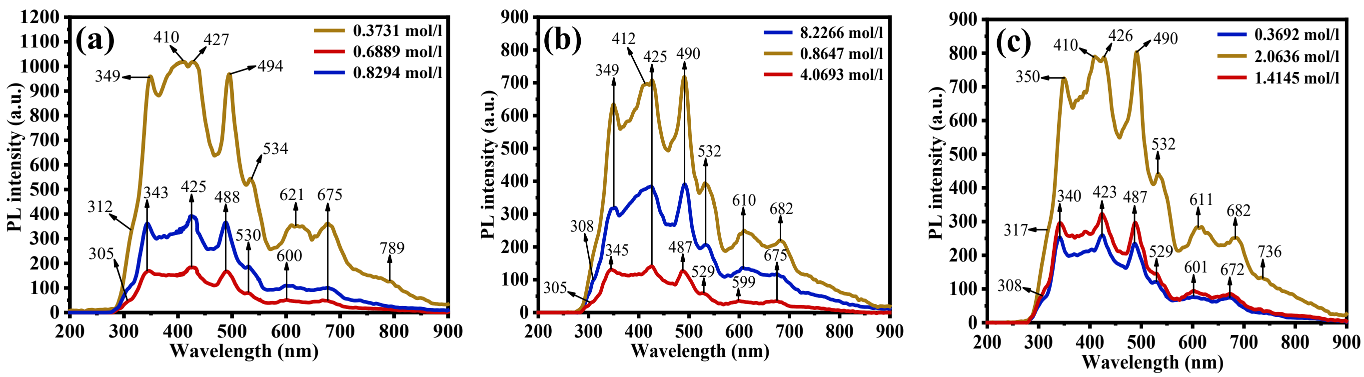

Figure 3.2: PL spectra of the silica particles at different concentrations of reactants: (a) TEOS concentrations, (b) H_2O concentrations, and (c) Ammonia concentrations,

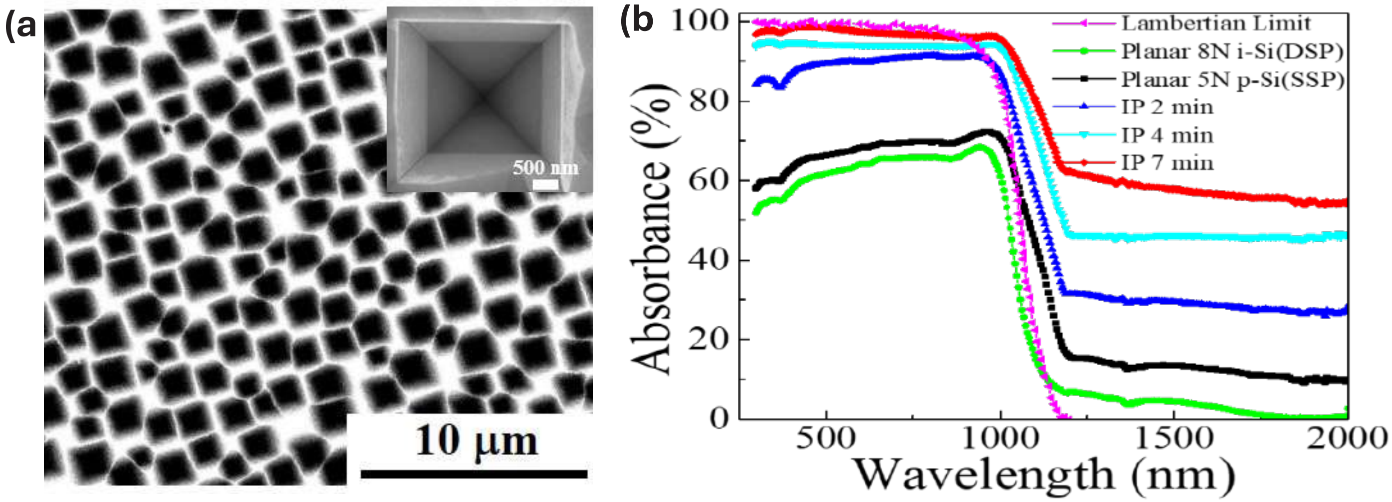

Figure 3.3: (a) Top-View FESEM image of inverted pyramid array pattern. Inset shows higher magnification top view image of one typical inverted pyramid. (b) diffuse reflectance spectra of planar Si and inverted pyramid arrays

particles was formed on the top surface of Si wafers. Then, reactive ion etching was done to introduce a controlled gap between silica particles by reducing their size. Then, a metal coating was done above the non-closed pack pattern. The metal touches the Si surface where Si particles were not there and other places left uncovered by the metal. After this, a lift off process was done to remove the silica particles, so that a metal mesh structure could be formed. Then, a controlled chemical etching was introduced to fabricate a periodic pattern of inverted pyramid structures. By varying the etching time (2–7 min) depth of the inverted pyramids was controlled.

The optical properties of the fabricated silicon inverse pyramid arrays were examined using diffused reflectance spectroscopy across the UV-VIS-NIR spectrum (300–2000 nm). Figure 3.3 (b) presents the diffused reflectance spectra of inverted pyramid arrays processed for different durations (IP-2 min, IP-4 min, and IP-7 min), alongside reference samples: planar 5N p-type silicon (single-side polished) and 8N intrinsic silicon (double-side polished). The planar 8N intrinsic silicon exhibited an average reflectance of 36.7% in the 300–1000 nm range, which increased to approximately 44% in the 1100–2000 nm range. Similarly, planar 5N p-type silicon showed average reflectance values of around 32.5% and 43.3% in the respective spectral ranges.

In contrast, the inverted pyramid arrays demonstrated a substantial reduction in reflectance. For the 300–1000 nm range, the average reflectance values were 10.5%, 5.8%, and 2.9% for 2 min, 4 min, and 7 min of etching, respectively. In the 1100–2000 nm range, these values were 34.9%, 20.3%, and 14.7%, respectively. This significant reduction in reflectance across the entire spectral range (300–2000 nm) confirms the enhanced light-trapping capability of the inverted pyramid structures, making them highly effective for photovoltaic and optoelectronic applications.

3.3 Synthesis of compound perovskite and its characterisation

In a related study, the compound perovskite $\{Pb(Mg_{1/3}Nb_{2/3})O_3\}_{1-x}\{PbTiO_3\}_x$(PMN-PT) single crystals were synthesized using a solid-state technique, and their structural and optical properties were investigated. X-ray diffraction patterns (Figure 3.4) confirmed a monoclinic structure for compositions with x = 0.1, 0.2, 0.3, and 0.4, showing reflection planes <100>, <110>, <111>, <200>, <210>, and <211>. The presence of prominent peaks indicates a dominant pyrochlore phase. As the $PbTiO_3$ content increases, lattice distortion becomes more significant, leading to noticeable modifications in the monoclinic symmetry of the PMN-PT structure.

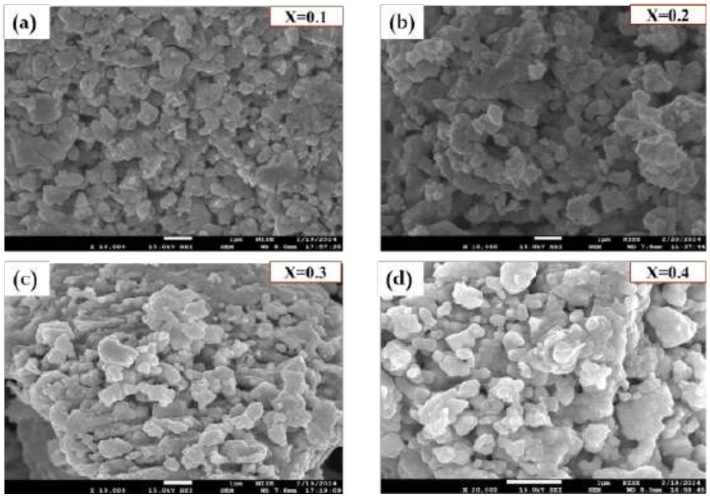

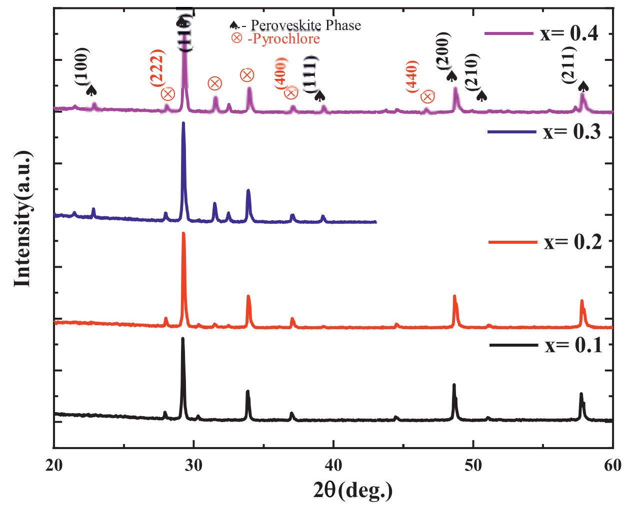

Figure 3.4: Room temperature X- ray diffractograms of $\{Pb(Mg_{1/3}Nb_{2/3})O_3\}_{1-x}\{PbTiO_3\}_x$

Figure 3.5: FESEM observations for $\{Pb(Mg_{1/3}Nb_{2/3})O_3\}_{1-x}\{PbTiO_3\}_x$ samples for x=0.1 to 0.4

The morphological analysis of the compound perovskite $\{Pb(Mg_{1/3}Nb_{2/3})O_3\}_{1-x}\{PbTiO_3\}_x$ reveals a clear variation in mean particle size with changing $PbTiO_3$ concentrations, as shown in Figure 3.5. At x = 0.1, the mean particle size is approximately 0.128 µm, increasing to 0.223 µm at x = 0.2. This growth in particle size is attributed to the incorporation of $PbTiO_3$ into the crystal lattice, which reduces the density of defects and enhances grain boundary mobility. In thin films, such particle growth can improve mechanical and electrical properties by reducing the number of grain boundaries, which often act as scattering centers for charge carriers or stress concentration points.

However, as the $PbTiO_3$ content increases further, the mean particle size decreases to 0.210 µm at x = 0.3 and further to 0.145 µm at x = 0.4. This reduction is likely due to $PbTiO_3$ atoms segregating to the grain boundaries, where they serve as pinning sites. These pinning sites hinder grain boundary movement during sintering, thereby restricting grain growth. As a result, the overall particle size diminishes.

The presence of smaller grains increases the number of grain boundaries, which can negatively impact properties such as dielectric strength and electrical conductivity. Grain boundaries may obstruct charge carrier mobility or act as sites for dielectric breakdown, ultimately affecting the performance of PMN-PT-based devices.

Figure 3.6 represents the FTIR spectra of $\{Pb(Mg_{1/3}Nb_{2/3})O_3\}_{1-x}\{PbTiO_3\}_x$ for x = 0.1 to 0.4, highlighting key vibrational modes associated with specific bonds in the material. The peak at 508 cm^{-1} is attributed to the flexural vibrations of Ti–O bonds within the TiO_6 octahedra, characteristic of the perovskite structure. The 598 cm^{-1} peak corresponds to the stretching vibrations of Nb–O bonds in the NbO_6 octahedra, indicating the presence of niobium in the lattice. A distinct peak at 859 cm^{-1} is linked to complex vibrational modes involving Pb–O bonds and possible interactions within the lead oxide environment. These FTIR features confirm the structural integrity and multi-element bonding nature of the PMN-PT compositions.

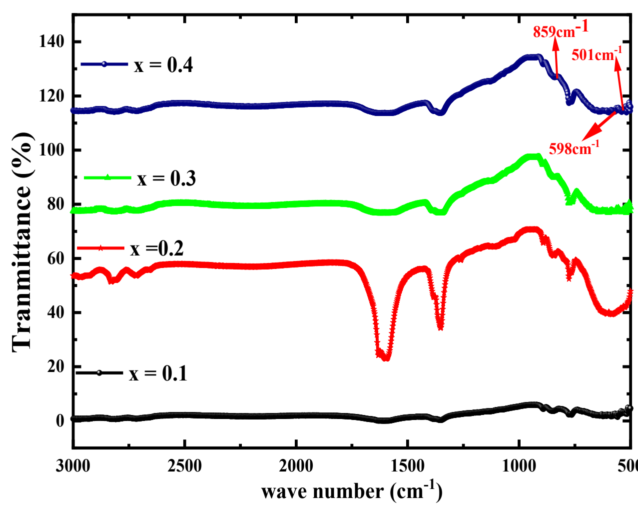

Figure 3.6: FTIR spectra of $\{Pb(Mg_{1/3}Nb_{2/3})O_3\}_{1-x}\{PbTiO_3)_x$

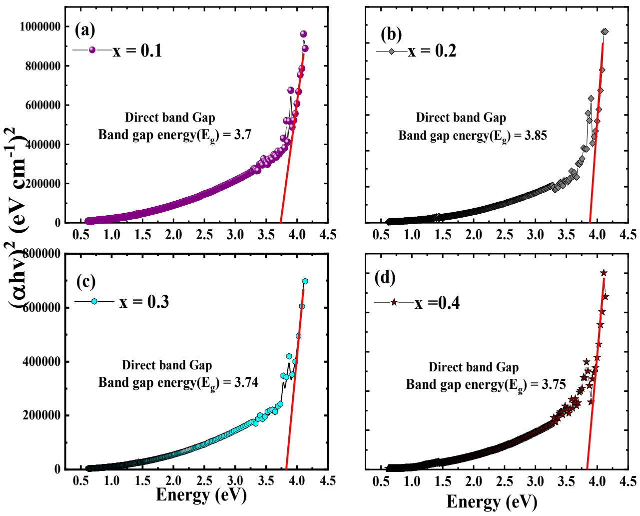

Figure 3.7: (a)-(d) Tauc plot for the $\{Pb(Mg_{1/3}Nb_{2/3})O_3\}_{1-x}\{PbTiO_3\}_x$

The optical band gap values of $\{Pb(Mg_{1/3}Nb_{2/3})O_3\}_{1-x}\{PbTiO_3\}_x$ thin films (x = 0.1, 0.2, 0.3, 0.4) were determined using the Tauc relation by plotting $(\alpha h\upsilon)^2$ versus photon energy, where α is the absorption coefficient determined from UV-Vis-NIR absorption spectra. The estimated band gaps were 3.70 eV, 3.85 eV, 3.74 eV, and 3.75 eV, respectively, as shown in Figure 3.7. These values were obtained by extrapolating the linear region of the Tauc plots.

3.4 Optimization of stabilization procedure of reference solar cell

A study has been done on different stabilization procedure of solar cell to be used as reference solar cell. We compared stabilization of solar cell with dark annealing, dark current biasing, and operating the solar cell at maximum power point (MPP) for multiple periodic durations under illumination. It has been observed that the typical time for stabilization of a solar cell in terms of power is more than 1000 hours of light soaking or dark current bias with a power loss of 0.37% and 0.36% for the respective methods. However, the stabilization procedure may also depend on the technology of the reference solar cell. All stabilization methods demonstrated sufficient potential for stabilizing c-Si solar devices for standardized power measurement. Figure 3.8 shows the dark I-V of the solar cell after applying different stresses.

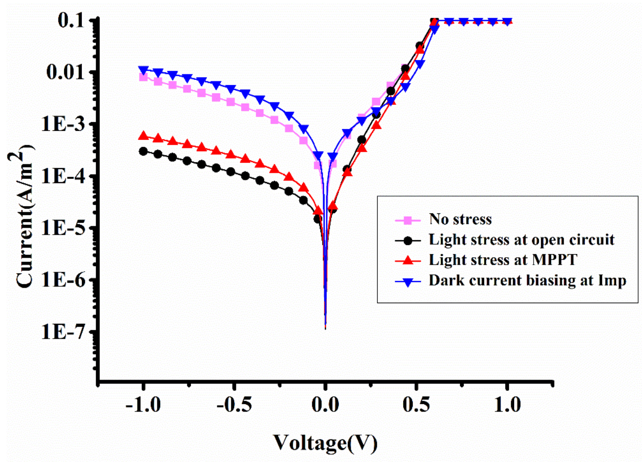

Figure 3.8: Dark I-V of solar cell with different stabilization procedure

3.5 Estimation & potential assessment of PV module waste in India

The rapid expansion of solar energy in India presents an emerging challenge regarding the management of photovoltaic module waste. As large-scale solar installations in India are about to reach the end of their 25–30-year lifespan, a significant volume of waste, including panels, mounting structures, and electronic components, is expected. This study aims to estimate the projected location-specific PV waste generation in India through 2047 by analyzing historical installation data from 2016–2022 and incorporating assumptions reported in the literature. A multi-faceted approach is employed, incorporating historical data analysis, growth trajectory modelling, and end-of-life projections based on panel degradation patterns. A solar panel weighing 0.672 kg/W_p was analyzed by removing each component and calculating its composition. The panel consists of 51.6% glass, 20.2% aluminum frames, 14.9% solar cells, 6.9% metal connections, 3.6% EVA & back sheet, and 2.1% junction boxes in terms of kg/W_p. The study provides state-wise projections of PV waste considering the component-wise weight/W_p, identifying Rajasthan, Karnataka, and Tamil Nadu as the largest contributors. By 2047, India is projected to generate approximately a cumulative total of 288 million tons of PV waste considering PV modules only. This highlights the urgent need for sustainable waste management and recycling solutions. This study's waste projection is based on assumptions considering components for glass to back sheet solar panels, panel failures, transport damage, and installation defects, which may not fully reflect real-world variations. Future research should incorporate real-time performance data, technology-specific analysis, and location-based projections for more accurate assessments. This research will help serve as a strategic guide for policymakers, industry stakeholders, and waste management authorities by informing capacity planning, policy development, and infrastructure investments. Figure 3.9 shows the cumulative component-wise waste generation in the top nine states of India by 2047.

3.6 Improved Performance Assessment of Bifacial PV Modules Using Modified Equivalent Irradiance Method

Assessing bifacial PV module performance is challenging due to variability in albedo and the lack of standardized performance metrics. Field-level analysis becomes further challenging when assessing the performance of bifacial PV modules. Currently, IEC TS 60904-1-2:2024 provides two standardized indoor measurement methods: dual-side illumination and the equivalent irradiance (GE) method. Through this research work, it has been demonstrated to what extent actual power deviates from the estimated power using the GE method as per IEC 60904-1-2. In this study, a bifacial module was measured under indoor conditions as per IEC 60904-1-2 to estimate the power and compared with the performance under outdoor conditions with various front and rear irradiance simultaneously. It was found that there is a deviation of around 60% at low irradiance and around 15% at higher levels (Figure 3.10). To address this issue and achieve accurate measurements, the formula was modified to account for various environmental factors, including spectral variations, the ratio of direct to diffuse irradiance, temperature fluctuations, and the Angle of Incidence (AoI). A direct and diffuse corrected equivalent irradiance calculation, based on IEC 61853-3, has been employed to overcome these challenges. This approach incorporates the influence of these critical parameters, leading to a substantial reduction in deviations over a wide range of irradiance levels, from low to high. The GE, Modified method enables a more precise evaluation of bifacial PV module performance under real-world outdoor conditions by aligning it more closely with indoor measurement results. This advancement is particularly valuable for the PV community, as it bridges the gap between indoor and outdoor performance assessments, providing a reliable framework for assessing the

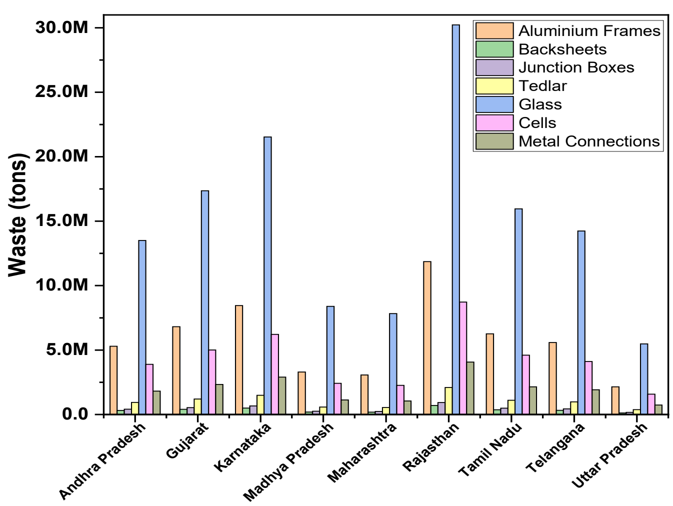

Figure 3.9: Cumulative component-wise waste generation in the top nine states of India by 2047

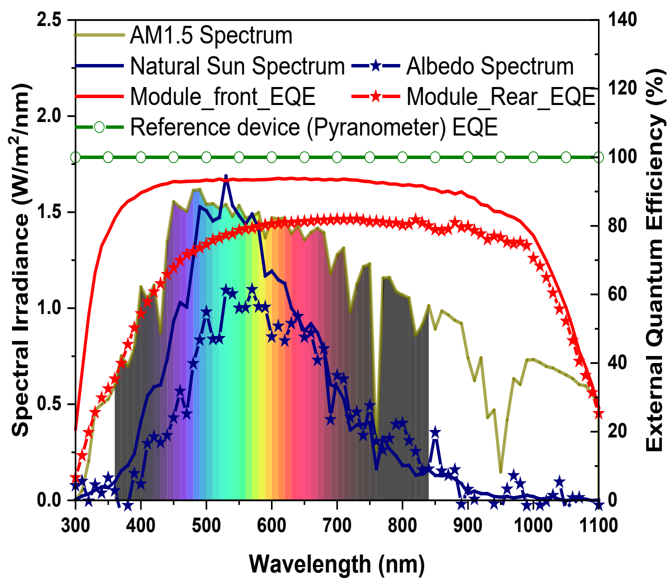

Figure 3.10: Spectral mismatch calculation

performance of bifacial PV modules. By capturing the complexities of outdoor operation, the GE, Modified method ensures robust performance estimation, aiding in the widespread adoption and integration of bifacial PV modules in real-world solar energy applications (Figure 3.11).

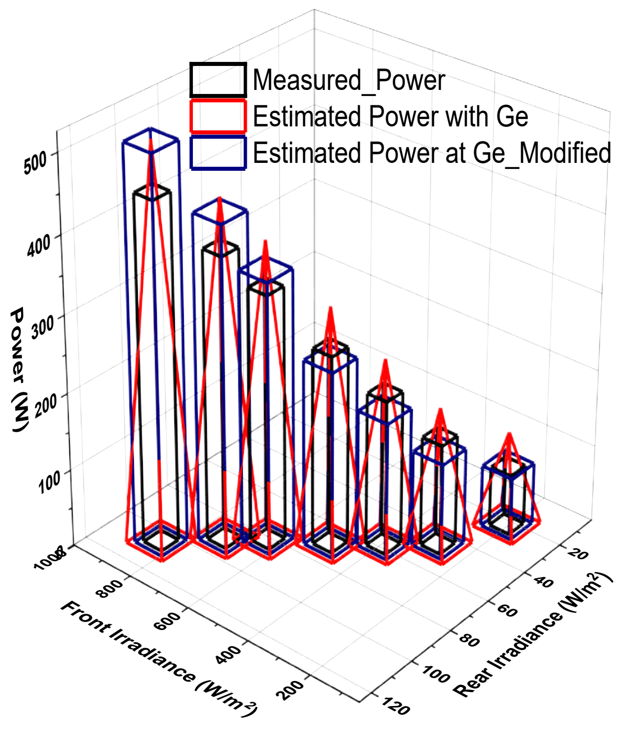

Figure 3.11: Deviation in measured Power with respect to GE and GE, Modified method

3.7 Design and Simulation of Agri-Voltaic Power Plant for Different Agro-Climatic Zones of India

NISE conducted a study on the design and simulation of agrivoltaic power plants for India's fifteen agro-climatic zones. For each zone, PV power plants were designed with different orientations, and simulations were conducted to determine the potential energy output and the size of the installations for 1 acre of land. Additionally, the Levelized Cost of Electricity (LCOE) for each zone was also calculated. This helps in evaluating the cost-effectiveness of these systems in different regions. The results provide valuable insights into how agrivoltaic systems can be optimized for specific regions in India with generation (kWh/kW$_p$/yr) and the approximate size for each acre of land availability. Simulation results show that a maximum energy of approximately 6,13,936 kWh/yr can be produced in the Western Dry Region using bifacial modules, which refers to an energy production of 327.04 kWh/acre of land. The minimum energy of approximately 2,64,364 kWh/yr can be produced in the Eastern Himalayan Region, which refers to an energy production of 193 kWh/acre of land. Figure 3.12 shows the energy yield and optimum tilt angle for

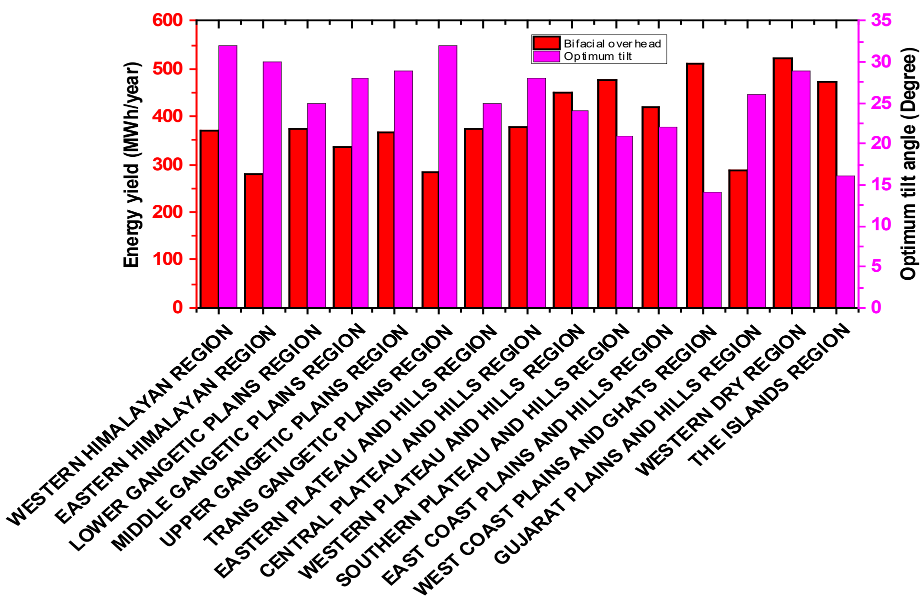

Figure 3.12: Energy yield and optimum tilt angle for overhead power plant

overhead AgriPV power plants for different agro-climatic zones.

3.8 Centre of Excellence (CoE) for Agri-PV

In FY 2024-25, the Centre of Excellence (CoE) for AgriPV at NISE undertook a series of impactful activities to advance the adoption and understanding of AgriPV systems in India. Key initiatives included the development of a dedicated AgriPV webpage and the creation of a two-page informative brochure to raise awareness among stakeholders. The CoE conducted an impact assessment of crops under AgriPV installations and developed a comprehensive crop suitability matrix. A set of India-specific guidelines for AgriPV systems was prepared to support standardized implementation. Field visits were carried out across six operational AgriPV sites in Maharashtra, Gujarat, Madhya Pradesh, and Delhi to document best practices and challenges of AgriPV systems under Indian conditions. The CoE organized five national webinars covering diverse themes, from technical design to policy frameworks, with participation from industry experts, developers, and farmers. Extensive farmer engagement was facilitated through PM-KUSUM awareness workshops held at multiple Krishi Vigyan Kendras (KVKs) across India, as well as through participation in the Krishi Udyog Samagam 2025 in Indore. Stakeholder consultations were held with key industry players and policymakers, resulting in a draft policy recommendation report, including a comparative analysis of AgriPV policies in various countries to guide national policy formulation.

3.9 Framework for re-use of Secondary life PV modules in distributed PV applications:

Re-use of secondary-life PV modules can play an important role in promoting a more secure, sustainable, and resource-efficient solar industry. A comprehensive framework has been developed for the re-use of secondary-life PV modules in distributed PV applications. This approach focuses on the effective identification, characterization, and repair (if required) of fielded PV modules. Implementing such a re-use strategy can significantly reduce the volume of end-of-life (EoL) modules and ease pressure on solar supply chains. However, user acceptance and financial feasibility are critical to the success of this initiative. Business case studies suggest that, for re-use to be attractive to end users, the modules should have a remaining service life of at least 10 years. To support widespread adoption, there is a need for advanced, cost-effective diagnostic and measurement tools that can reliably assess module health and performance, ensuring the economic viability of secondary use. Figure 3.13 shows the different parameters considered for estimating the cost of PV module for secondary use.

3.10 Floating Solar PV Potential Assessment

Floating Solar Photovoltaic (FSPV) systems offer a practical solution by utilising water bodies for solar energy generation, thereby reducing the stress on land resources. To address these challenges and support India’s renewable energy goals, the NISE has developed a robust methodology for assessing and quantifying the potential of floating solar PV installations across the country.

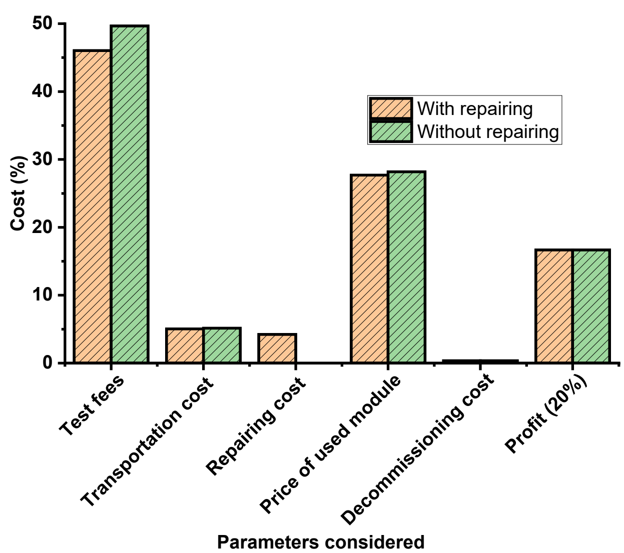

Figure 3.13: Distribution of different parameters used for cost estimation of PV module for secondary use

NISE adopts a data-driven analytical approach, leveraging high-resolution GeoBase data to ensure precision and reliability. The assessment included an in-depth analysis of various parameters, including water bodies, water availability (Seasonality) and bathymetry (Water depth) as well as the parameters used in ground-mounted solar potential assessment, such as road network, transmission substations and solar irradiance data to ensure optimal site selection, efficiency, and sustainability to deliver a high-resolution assessment of feasible sites. The methodology considered for the floating solar potential of India is provided in Figure 3.14. The procedure followed is explained using a case study to overcome the visibility of these features on the map.

Case Study of Floating Solar Water Body Feasible Area Estimation

Due to the limited visibility of hydro lakes on the Indian map, the methodology for evaluating the floating solar potential has been demonstrated using the Hirakud Reservoir as a representative case study. A systematic geospatial analysis was undertaken to identify feasible areas for photovoltaic installation. The assessment commenced with the selection of the Hirakud Reservoir from hydrological datasets, delineating its spatial extent to serve as the analytical foundation, as illustrated in Figure 3.15. Subsequently, a temporal analysis of water availability was conducted by processing 12 months of seasonality data derived from the Global Surface Water (GSW) dataset, ensuring year-round water presence within the reservoir, as depicted in Figure 3.16.

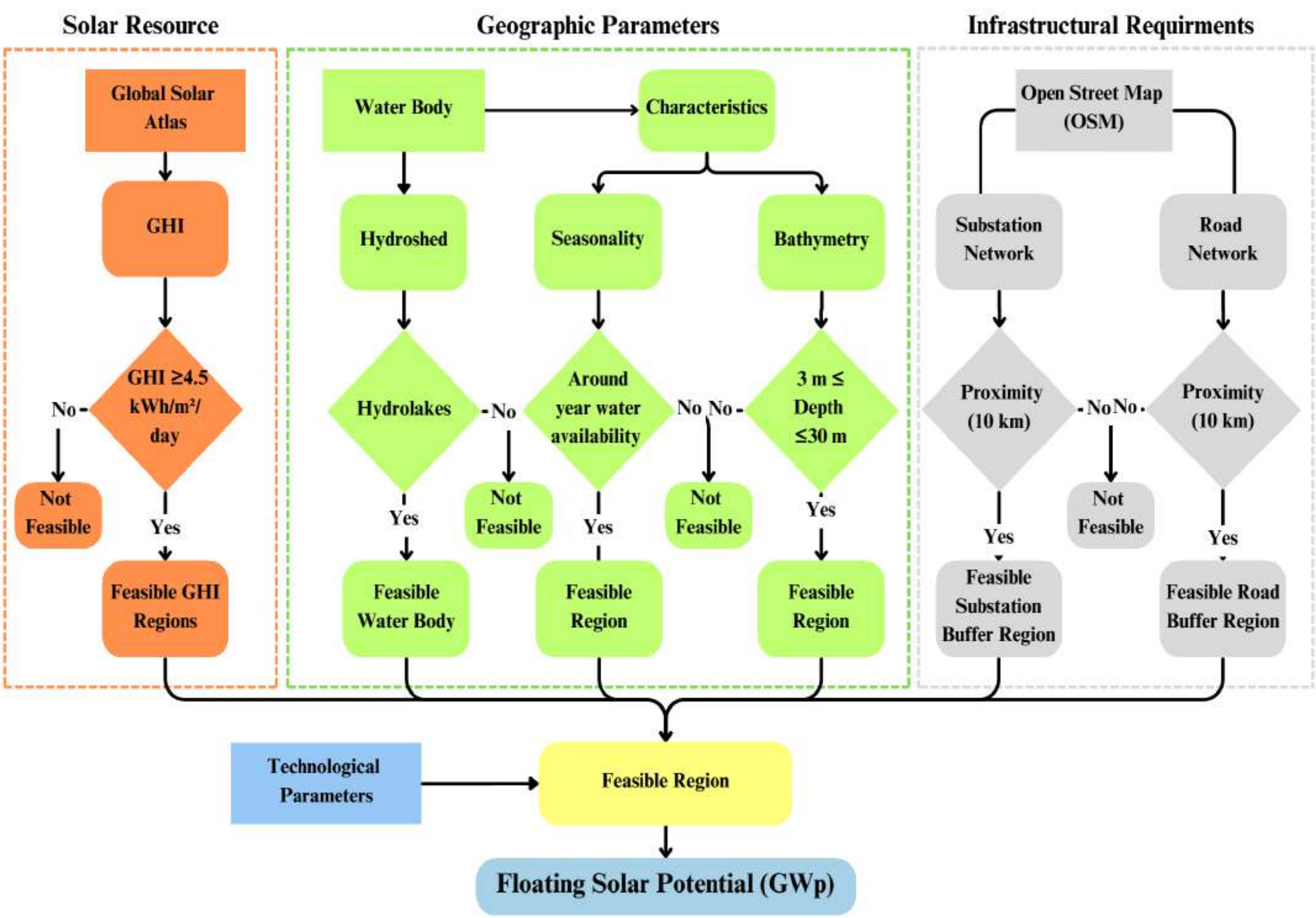

Figure 3.14: Flowchart of the methodology used for the floating solar potential assessment

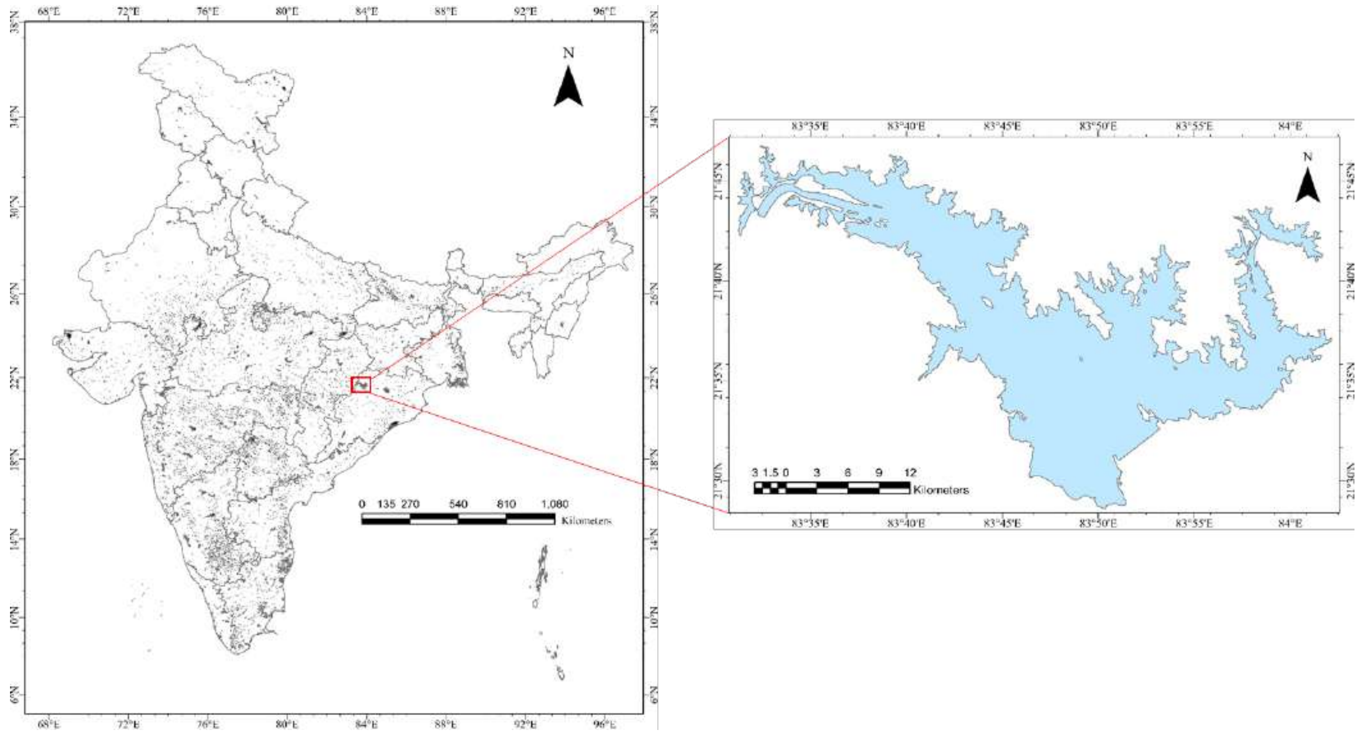

Figure 3.15: Hirakud Reservoir from the hydrological datasets

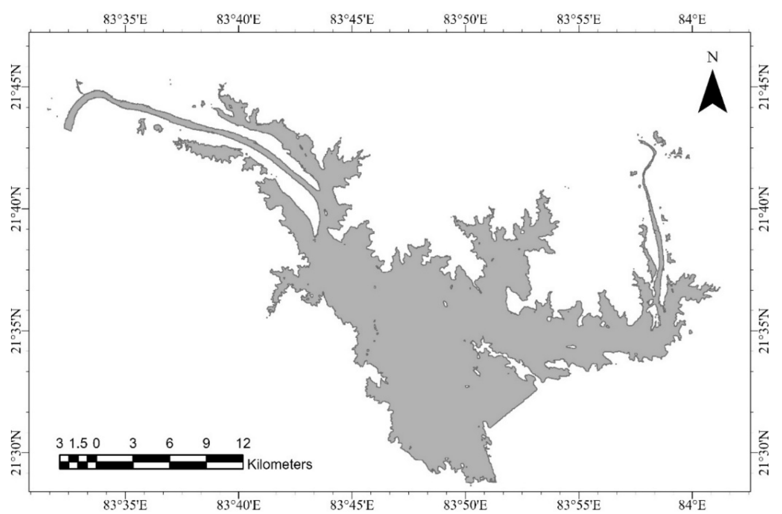

Figure 3.16: The graphical presentation of seasonality of Hirakud reservoir sourced from Global Surface Water dataset

Following this hydrological assessment, bathymetric data obtained from the GLOBathy dataset were integrated to determine water depths ranging from 3 to 30 metres, which are considered optimal for the deployment of floating solar systems, as shown in Figure 3.17. Areas with depths shallower than 3 metres were excluded to mitigate risks related to structural stability, while regions exceeding 30 metres were disregarded due to complexities associated with anchoring and cost implications.

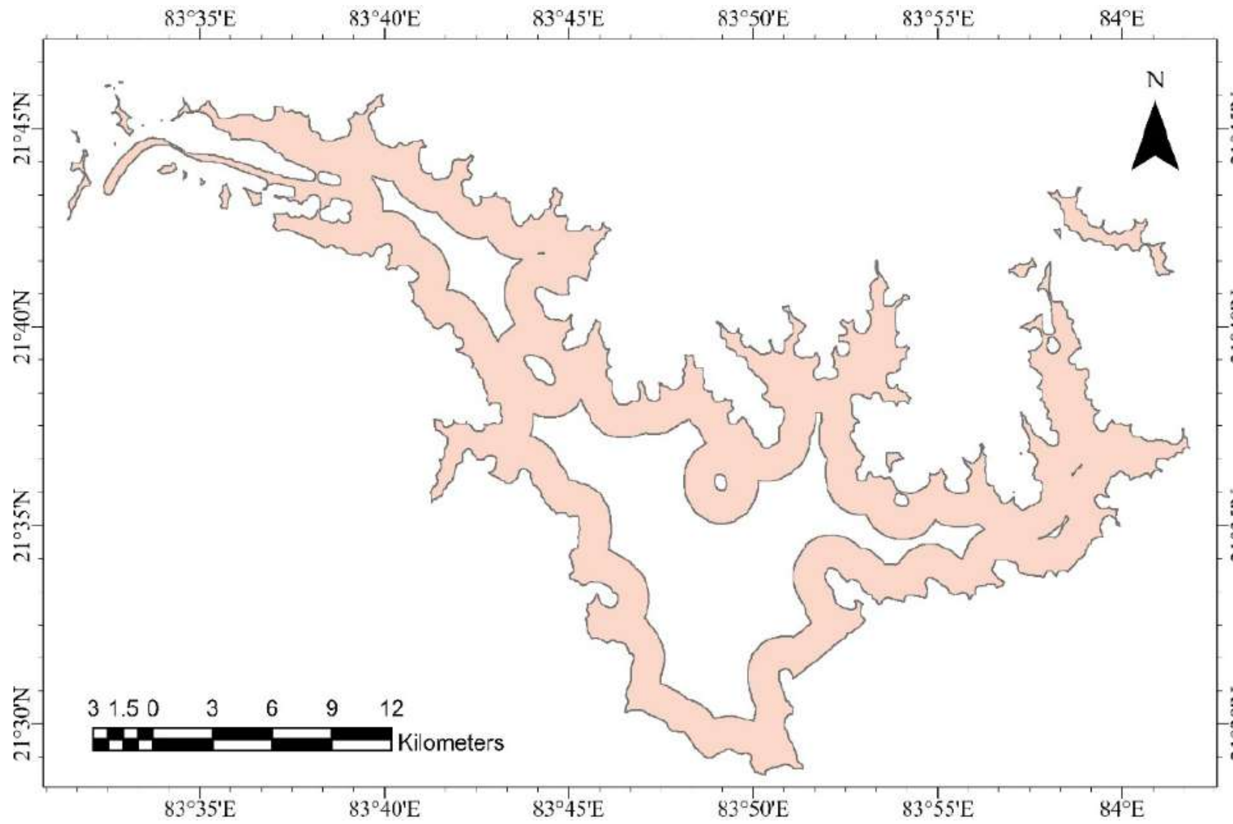

Figure 3.17: The graphical presentation of bathymetry of Hirakud reservoir sourced from GLOBathy

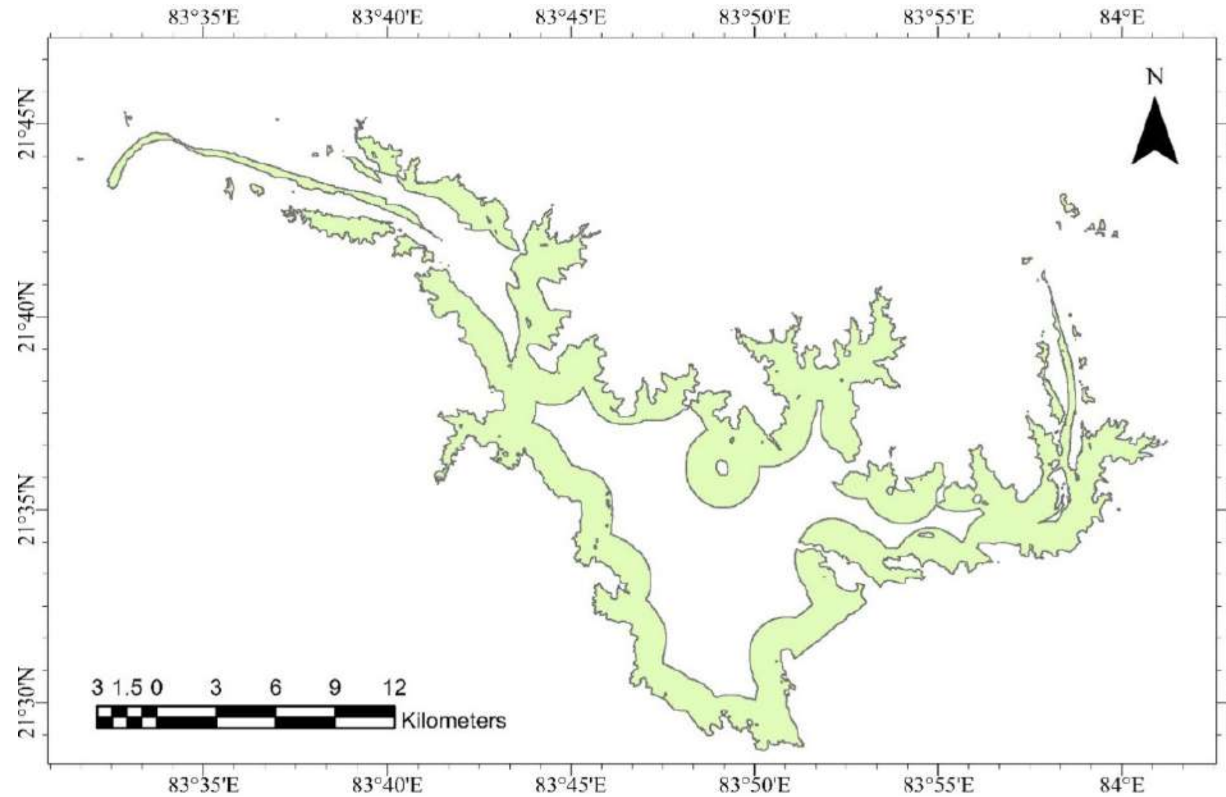

Figure 3.18: Feasible sites of Hirakud for Floating PV installation

Combining the given parameters encompassing Hydrolake, Seasonality, and Bathymetry the feasible sites for the floating solar are identified and are shown in Figure 3.18. This multi-criteria assessment ensured the selection of areas that are technically feasible, economically viable, and environmentally sustainable for floating PV installations. The analysis of the Hirakud Reservoir revealed that out of the total water surface area of 499.48 km^2 approximately 204.53 km^2 met the defined criteria for year-round water availability and suitable depth (3 to 30 metres).

3.11 Solar cooking with Energy Storage System

To promote sustainable and clean energy technologies, an Indoor Solar Cooking System integrated with Thermal Energy Storage has been developed to enable reliable, round-the-clock cooking. The system harnesses solar energy during daylight hours for direct cooking applications, while simultaneously storing excess thermal energy in a dedicated storage unit. This stored heat can then be utilized during off-peak hours or in the absence of sunlight, ensuring uninterrupted cooking. The technology is particularly suited for domestic use in areas with inconsistent energy supply and aims to reduce dependence on conventional cooking fuels.

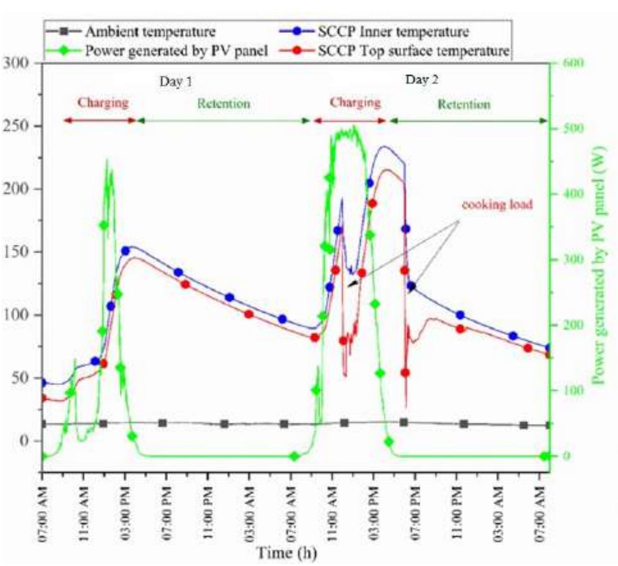

Figure 3.19: Cooking performed in the Indoor Solar Cooking System

The system has successfully completed the design and laboratory testing phase, and pilot deployments are being planned to evaluate field performance and user acceptance. Figure 3.19 represents the charging and retention periods along with cooking load represented by dip in temperature of the solar cooker.

3.12 Solar Cabin with Thermal Energy Storage

The division is actively engaged in the development of an innovative solar space heating system designed for residential and institutional use in the cold climatic zones of the Himalayan region. The system uses solar photovoltaic panels to generate electricity, which is converted into thermal energy and stored in a cost-effective, sand-based thermal battery. This stored heat is used to maintain indoor warmth during night-time and low-sunlight conditions.

To enhance performance and adaptability, the division is also working on multiple configurations of the sand battery. The system offers a zero-emission, sustainable alternative to conventional heating methods, with prototype development underway and field demonstrations planned.

Figure 3.20 represents the variation of solar intensity and temperature of thermal energy storage material, cabin, and ambient in a day.

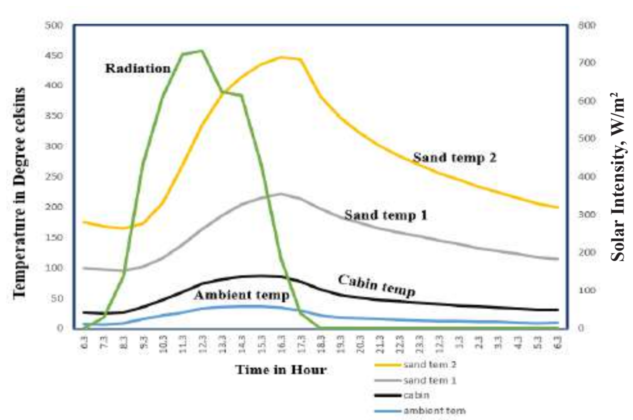

Figure 3.20: Performance Graph of various temperature and radiation during testing

3.13 Instant Solar Geyser

The Solar Thermal Division has developed a novel instant water geyser integrated thermal energy storage to enable consistent hot water supply using solar energy. Unlike conventional geysers, which take some time to heat water, this system provides hot water instantly as and when required.

By incorporating thermal energy storage into the geyser, the system addresses the intermittent nature of solar energy. The system uses solar PV panels for electricity generation which is then stored in the TES using centrally placed heating element housed within the well-insulated metallic tank. The thermal energy from the TES is transferred to the input cold water (Figure 3.21).

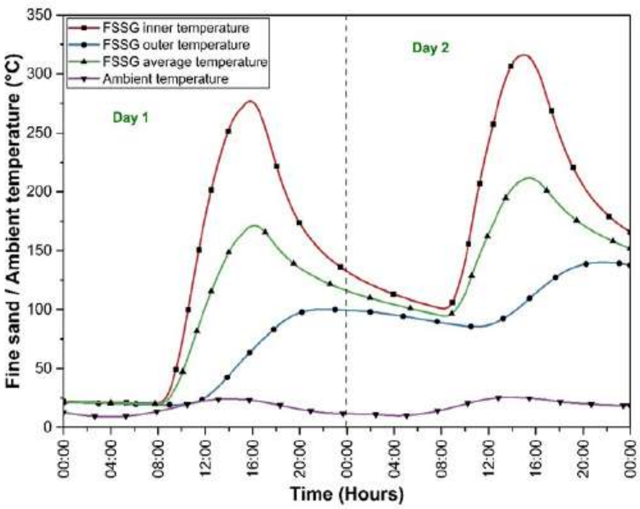

Figure 3.21: Temperature variation of fine sand and ambient during the charging operation.

This configuration, with TES as the heat transfer and storage medium, ensures efficient energy utilization and a sustainable solution for instant hot water supply, even when solar energy is not directly available.

3.14 Solar-Powered Micro-Irrigation: Field Study and Outcomes

To promote sustainable water management and climate-resilient agriculture, NISE conducted a study to assess the feasibility of solar-powered micro-irrigation systems utilizing surface water sources such as shallow ponds and farm tanks. A solar-powered water distribution unit was integrated with a drip irrigation network. Water was drawn from a water tank and system operated twice daily for 43 minutes, resulting in 86 minutes of irrigation per day.

A study was conducted to evaluate the feasibility and functional reliability of a portable, solar-powered micro-irrigation system using surface water sources such as shallow ponds or farm tanks. System operated effectively with a single solar panel, delivering consistent water output for drip irrigation under real-world field conditions. This validates the potential of the setup as a low-cost, mobile solution for small-scale farmers, especially in areas with limited access to groundwater. While crop yield was recorded, the primary objective was to assess whether the technology could function efficiently and support irrigation needs. The results affirm that such systems can significantly reduce water consumption and offer a sustainable alternative for decentralized irrigation.

3.15 Reliability & Performance Evaluation of Solar Water Pumping System

Solar water pumps are deployed in varied geographic and climatic zones across India and hence these systems must function reliably under diverse water qualities, including saline, muddy, and high-particulate content conditions. NISE has developed a state-of-the-art test R&D facility to evaluate the reliability, durability, and performance of AC/DC solar water pumping systems ranging from 1 hp to 10 hp and capable of handling total dynamic head up to 200 metres (Figure 3.22). The test facility includes two dedicated test slots (2" and 3") accommodating muddy and saline water with a pH range of 7.5 to 8.4 and equipped with advanced instruments to assess key performance indicators such as flow rate, pressure head, input power, temperature profiles, and mechanical wear, enabling a thorough analysis of system durability and reliability. This initiative is crucial for benchmarking product quality and ensuring suitability for diverse Indian field conditions by ensuring:

Figure 3.22: Reliability & Performance Evaluation of Solar Water Pumping System Reliability test set up at NISE

- Standardized performance verification under controlled but realistic conditions.
- Long-term reliability data for components and different materials.
- Improved decision-making for technology selection and policy formulation.
- Evaluation of material performance, especially for pump wetted parts made from Cast Iron (CI) and Stainless Steel (SS).

3.16 R&D Outcomes

Patent Filed

1. A Solar Dryer (Indian Patent Application No. 202411060884)

Publications

Journals

1. "Synthesis of sputtered self-catalytic indium tin oxide nanorods for photovoltaic application," S. Dhar, S. Mandal, G. Das, W Li, S. Mukherjee, C. Banerjee, H. Saha, and A.K. Barua: Journal of Alloys and Compounds, Vol. 1004, 175757, 2024, doi.org/10.1016/j.jallcom.2024.175757.
2. "Experimental investigation and energy-exergy analysis of indirect liquid jaggery-making system based on parabolic dish concentrator," V. Kumar, C. M. Chandrashekara, and A. Yadav: International Journal of Exergy, vol. 43, no. 1, pp. 59–80, 2024, doi: 10.1504/IJEX.2024.136452.
3. "Water generation through desiccant using novel-designed solar still coupled with heat pipe vacuum tube collector: An experimental observation," R. Srivastava, C. M. Chandrashekara, and A. Yadav: Heat Transfer, vol. 53, no. 4, pp. 1770–1789, 2024, doi: 10.1002/htj.23013.
4. "Experimental comparison of solar drying based on evacuated tube collector with desiccant drying for dehydrating potato and ginger," S. Vyas, P. Singh, H. Agrawal, G. Vishwakarma, and A. Yadav: Heat Transfer, vol. 53, no. 4, pp. 2128–2147, Jun. 2024. doi: 10.1002/htj.23030.
5. "Fabrication and experimental investigation of a novel sensible heat storage system for indoor solar cooking," V. Vipin, N. K. Singh, and A. Yadav: Journal of Energy Storage, vol. 117, 116201, 2025, doi: 10.1016/j.est.2025.116201.
6. "Development and performance evaluation of a photovoltaic-integrated thermic solar geyser for domestic water heating," D. K. Saini, C. Muniyappa, and A. Yadav: Thermal Science and Engineering Progress, vol. 62, 103642, 2025, doi: 10.1016/j.tsep.2025.103642.
7. "Experimental investigation of a novel photovoltaic based solar geyser with sensible

heat storage," D. K. Saini, C. Muniyappa, and A. Yadav, Journal of Energy Storage, vol. 121, 116570, 2025, doi: 10.1016/j.est.2025.116570.

8. "Thermal analysis of a rectangular latent heat storage unit with stearic acid/paraffin wax composite PCM for solar thermal energy storage systems," D. K. Saini, C. Muniyappa, and A. Yadav: Energy Sources, Part A: Recovery, Utilization, and Environmental Effects, vol. 47, no. 1, pp. 4279–4296, 2025, doi: 10.1080/15567036.2025.2460644.

9. "Thermal performance analysis of a fine sand solar geyser integrated with photovoltaic technology," D. K. Saini, C. Muniyappa, A. Yadav, and S. Zaphar: Energy Sources, Part A: Recovery, Utilization, and Environmental Effects, vol. 47, no. 1, pp. 12247–12266, 2025, doi: 10.1080/15567036.2025.2507096.

10. "Solar photovoltaic water heater with integrated thermal storage: an experimental evaluation," D. K. Saini, C. Muniyappa, and A. Yadav: Journal of Thermal Analysis and Calorimetry, 2025, doi: 10.1007/s10973-025-14490-4.

11. "Experimental analysis of stearic acid/paraffin wax composite PCM in a rectangular thermal energy storage unit integrated with heat pipe vacuum tube solar collector," D. K. Saini, C. Muniyappa, and A. Yadav: Journal of Thermal Analysis and Calorimetry, vol. 150, pp. 11049–11066, 2025, doi.org/10.1007/s10973-025-14447-7.

12. "Tailoring the morphological and optical properties of monodisperse silica, "A. Saini, H. Negi, S. K. Srivastava, P. Pathi, R. Yadav, M. Dutta, Journal of Sol-Gel Science and Technology, 113 (2025) 252-265

13. "A spectroscopic ellipsometry study of TiO_2:ZrO_2 on TiN/Si thin films prepared by Chemical Beam Vapor Deposition," P. Agnihotri, A. Verma, A. Saini, R. Rani, W. Maudez, E. Wagner, G. Benvenuti, C. Banerjee, M. Dutta, R. Rai, Surface and Interface Analysis 56 (11), (2024) 808-816.

14. "Oxygen-mediated defect evolution and interface analysis of MoO_x/n-Si devices," A. Kumar, S. Tomer, T. Fix, M. Dutta, S. K. Srivastava, P. Pathi, Journal of Physics D: Applied Physics 57 (2024) 505105

15. "Lithography-Free Method to Synthesize Quasiperiodic Silicon Inverted-Pyramid Arrays: A Broadband Light Trapper for High-Efficiency Thin Silicon Solar Cells," A. Kumar, D. Rani, A. Saini, N. Joshi, R. K. Varma, M. Dutta, A. Samanta, Solar RRL 8 (9), (2024) 2400014

16. "Effectual visible-driven photocatalytic performances on brilliant green dye by reduced graphene oxide–zinc oxide nanocomposite," P. Yadav, I. Kapil, M. Dutta, A. Bhaduri, Ionics 30 (2024) 2927-2937

17. "Investigation of dielectric transitions and impedance behavior in solid solutions of (1-x) $K_{0\cdot41}Na_{0\cdot59}Nb_{0\cdot959}Sb_{0\cdot041}O_3$ - x($Bi_{0\cdot5}K_{0\cdot5}TiO_3$), synthesized by solid state reaction method," R. Rai, P. Agnihotri, S. Kumari, M. Dutta, Journal of the Australian Ceramic Society, (2024).

18. "Nanoscale Effects in the Room-Temperature UV–Visible Photoluminescence from Silica Particles and Its Cancer Cell Imaging," D. Rani, D. Singh, A. Kumar, M. Dhiman, A. Saini, P. Biswas, R. Rachana, P. Roy, M. Dutta, A. Samanta, Bioconjugate Chemistry 36 (2025) 203-215.

19. "Study on Reliability of Field Aged Photovoltaic Connectors," K. Kapoor, M. Eswaramoorthy, D. Goyal, P.G. Nikhil: Maintenance and Reliability, Vol. 27 (2025), Issue 3.

20. "Techno–economic and environmental impact analysis of electric two-wheeler batteries in India," A. Gupta, D. Bose, S. Tiwari, V. Sharma, J. Prakash, Clean Energy 8(3) (2024), 147–156.

Conference

1. "Enhanced Absorption for Solar Cell Applications in Lead Free $CsSnI_3$ Perovskite by Embedding Plasmonic Nano-Octahedra," S. Tiwari, J. P. Singh and Y. Sharma, International Conference on Sustainable Power & Energy (ICSPE), Raigarh, India, 2024, pp. 1-5, doi: 10.1109/ICSPE62629.2024.10924368.
2. "Plasmonic Solar Cells: Mechanism and Fabrication Techniques," S. Tiwari, J. P. Singh, and Y. Sharma, 5th International Conference on Smart Electronics and Communication (ICOSEC), Trichy, India, 2024, pp. 21-28, doi: 10.1109/ICOSEC61587.2024.10722182.
3. "Reliability analysis of VRLA Batteries Using Failure Mode and Effects Analysis (FMEA) Technique for hot and Semi-Arid Indian Climatic Condition," D. Bose, S. Tiwari, A. Gupta, B. Bora, Proc 3rd IEEE Int Conf Power Electron Intell Control Energy Syst ICPEICES 2024. 2024; 773–778.
4. "Secondary Batteries for Sustainable Energy: A Comprehensive Review of the Indian Landscape," D. Bose, A. Gupta, S. Tiwari, D. Yadav, V. Sharma, Proc. Int Conf Soc Sustain Innov Technol Eng SASI-ITE, 2024; 413–417.
5. "Prediction of cavitation using machine learning techniques on centrifugal pump," C. Stephen, V. Guguloth, K. Sivasailam, Y. Gu, R. Parmar and C. Banerjee, Journal of Physics: Conference Series, 8th International Conference on Pumps and Fans, Yangzhou, China, Volume 2854, 2024, 1742-6596.

Book Chapter

1. "Numerical Simulation Studies on CdTe-Based Solar Cells," A. Rani, M. Dutta, C. Shekhar, A. Bhaduri, Page 22-35 (2024), Book title: Eco-Materials and Green Energy for a Sustainable Future, CRC Press